S-Doped MoP Nanoporous Layer Towards High-Efficiency Hydrogen Evolution in pH-Universal Electrolyte

Kun Liang[1], Srimanta Pakhira[2,3,4,8], Zhenzhong Yang[5], A. Nijamudheen [2,3,4], Licheng Ju[1], Maoyu Wang[6], Carlos I. Aguirre-Velez[2,3,4], George E. Sterbinsky[7], Yingge Du[5], Zhenxing Feng[6,], Jose L. Mendoza-Cortes[2,3,4,*], Yang Yang[1,*]*

[1]*NanoScience Technology Center, Department of Materials Science and Engineering, University of Central Florida, Orlando FL 32826, USA*

[2]*Department of Chemical & Biomedical Engineering, Florida A&M University, and Florida State University, Joint College of Engineering, Tallahassee FL, 32310, USA.*

[3]*Department of Physics, Scientific Computing, Materials Science and Engineering, High-Performance Material Institute, Florida State University, Tallahassee FL, 32310, USA.*

[4]*Condensed Matter Theory, National High Magnetic Field Laboratory, Florida State University, Tallahassee FL, 32310, USA*

[5]*Physical and Computational Sciences Directorate, Pacific Northwest National Laboratory, Richland WA, 99352, USA*

[6]*School of Chemical, Biological, and Environmental Engineering, Oregon State University, Corvallis OR, 97331, USA*

[7]*Advanced Photon Source, Argonne National Laboratory, Argonne IL, 60439, USA*

[8]*Discipline of Metallurgy Engineering and Materials Science, Indian Institute of Technology Indore, Simrol, Indore-453552, Madhya Pradesh, India.*

*E-mail: Yang.Yang@ucf.edu; mendoza@eng.famu.fsu.edu; zhenxing.feng@oregonstate.edu

ABSTRACT: In this study, we report a non-precious metal catalyst for high-efficiency hydrogen evolution reaction (HER). A self-organized S-doped MoP nanoporous layer (S-MoP NPL) is achieved through a facile electrochemical anodic process and a two-step chemical vapor deposition treatment, which was directly used as a binder-free catalyst for HER in pH-universal electrolytes. S-MoP NPL exhibits HER behavior with a low overpotential of 86 mV at 10 mA cm^{-1} and low Tafel slope of 34 mV dec^{-1} in acidic solution. Moreover, S-MoP NPL also shows high HER activity in basic and neutral electrolytes. Density functional theory (DFT) computations were carried out to support our experiment. The calculations show that the H_2 formation (via Volmer−Heyrovsky mechanism) from the reaction of a metal (Mo) absorbed hydride with a solvated proton is favored over S-MoP than MoS_2. Both experimental and computational studies demonstrate that the extraordinary HER activity and stability performance displayed by a MoP catalyst can be enhanced by S-doping, opening up a promising paradigm for the conscious design of high-performance non-precious metal catalyst for hydrogen generation.

Keywords: MoP; S-doping; nanoporous; pH-universal; hydrogen evolution

TOC

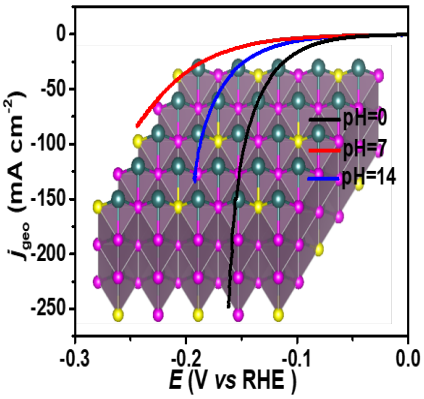

INTRODUCTION

Research development of advanced materials for renewable energy applications has recently attracted considerable attention.[1-4] As a clean energy, hydrogen shows great promise as an alternative to fossil fuels, owing to high energy density and environment-friendly. Currently, water electrolysis is a viable way to generate high-purity hydrogen, compared to traditional ways to produce low-purity hydrogen by means of methane oxidation and pyrolysis of hydrocarbons, which require further purification. However, developing high-efficiency and low-cost catalysts toward the hydrogen evolution reaction (HER) still remains a great challenge. By far, Pt is well-known as the most effective catalyst for HER and delivers very small overpotentials in an acidic electrolyte, but the large-scale application is impeded by the scarcity and high-cost associated with precious metals.[5] Therefore, it is highly desirable to replace precious metal catalysts with inexpensive and high-efficiency non-precious metal catalysts in a pH-universal electrolyte for HER.

Transition metal phosphides (TMPs), e.g. MoP, present high electronic conductivity, which is beneficial for promoting many electrochemical reactions such as hydrogenation, hydrodenitrogenation, and hydrodesulfurization (HDS). Essentially, HER and HDS undergo similar kinetic processes that reversibly bind hydrogen to the catalyst, therefore it is conceivable that MoP can act as a catalyst for HER.[6] Recent studies show that anion doping plays a critical role in further enhancing the electrocatalytic HER performance of MoP.[7-8] For example, an enriched number of electrochemically active sites can be achieved by coordinating MoP with a more electronegative S dopant, which ultimately renders a higher positive current density on the adjacent MoP catalyst.[9] Additionally, recent investigations suggest a synergic effect between P and S anions within catalysts, further demonstrating S-doped MoP as a promising high-

performance HER catalyst. Jaramillo *et al.* introduced S into the surface of MoP to produce a MoP|S catalyst, which is more active than those of pure S or pure P, owing to synergistic effects between S and P,[10] but in this report the S content was unknown. Similarly, Tour *et al.* reported an improved HER activity through the formation of a $MoS_{0.94}P_{0.53}$ solid solution, which shows that the HER activity can be further enhanced by increasing the surface area of the solid solution.[11] Furthermore, Fu *et al.* designed hierarchical flower-like MoS_2@MoP core-shell heterojunctions as HER catalyst, showing excellent electrocatalytic activity over a broad pH range. The as-prepared electrode exhibited varying HER catalytic activity by tuning phosphatization (P/S ratio).[12] The presence of S dopants could enhance catalyst-electrolyte interactions, reducing the work function and improving the electron transfer from the catalyst to electrolyte.[13-15] Above all, HER activity can be significantly promoted by doping S into MoP. Thus, the previous results showed excellent performance with either high S content or composite of MoS_2 and MoP. However, the small amount of S content (under 10 at%) doping in MoP has not been investigated in-depth yet. Generally, HER catalysts are derived from powder materials that need to be fixed onto a glassy carbon electrode or conductive current collector for catalysis. This can cause negative interactions between the catalyst and support constituents that will greatly affect catalytic performance and interfere with the identification of electrocatalytically active materials in a composite system. As a solution to the aforementioned issues, a binder-free Mo-based electrode combined with P and S anions could serve as an ideal interference-free platform for in-depth experimental, spectroscopy and theoretical/computational studies of S-doped MoP catalyst for HER. This can serve as a basic comprehension of the catalytic mechanism and develop the next generation HER catalysts.

In this work, a facile electrochemical anodic treatment was combined with a two-step

chemical vapor deposition (CVD) process to develop S-doped MoP nanoporous layer (S-MoP NPL), which was directly used as a binder-free catalyst for HER in pH-universal electrolytes. The porous morphology created by anodization treatment promotes proton transport and hydrogen adsorption, enhancing electron transfer efficiency. For an in-depth understanding of the synergic effects between S and P in S-MoP NPL, experimental, spectroscopic, and computational studies were performed to investigate the S-doping (concentration under 10 at%) effect on the HER activity of MoP. The presence of S dopant decreases the free energy of hydrogen adsorption and the hydrogen binding energy in electrolytes with different pH. Moreover, the presence of S dopant could enhance the interaction between catalyst and electrolyte, improving electrochemical activity. The 2D layer structure of MoS_2, MoP and S-doped MoP (i.e. MoSP) materials and their band structure and density of states (DOS) are investigated by employing the periodic dispersion-corrected DFT (i.e. DFT-D; here B3LYP-D2). The HER electrocatalytic performance was further explored by hybrid DFT-D method considering a model system. The present computational or theoretical process verified the HER kinetics mechanisms by simulating the activation barrier energies, and the relevance to their band gap and DOS of the HER in the presence of the aforementioned MoS_2, MoP and S-doped MoP 2D layer structure materials. Particularly, we have therotically analyzed and investigated the reaction mechanism of how the S-doped MoP's HER activation energy barrier is reduced after reducing S atoms doped in the MoP layer.

RESULTS AND DISCUSSION

A representative synthesis process is schematically displayed in Figure 1a (for more details see Experimental details in Supporting Information). Molybdenum foil was employed to anodically grow the MoO_3 NPL with a thickness of less than 1 μm (Figure 1b), which is

rationally designed to minimize electrode resistance and facilitate the electron/ion diffusion.[16-18] To convert MoO_3 NPL to S-doped MoP NPL, subsequent phosphorylation and sulfuration treatments were carried out. From the scanning electron microscopy (SEM) images (Figure 1c, 1d, S1), a self-organized NPL can be found without fracture and collapse after a two-step CVD treatment, where nanopore diameter is distributed between 50-80 nm, revealing a hierarchically mesoporous structure. As exhibited in Figure S2, it is found that P and S uniformly distributed across the entire layer.

The morphology and structure of S-doped MoP NPL were investigated by transmission electron microscopy (TEM, Figure S3). A porous architecture, similar to the structure detected by the top-view SEM image, was observed. High-resolution TEM (HRTEM) was employed to verify the lattice fringes within the NPL, as shown in Figure 1e. Two different lattice structure with *d*-spacings of 0.32 and 0.28 nm were found, corresponding to (001) and (100) planes of MoP.[19-20] Presence of a MoS_2 lattice fringe (100) with *d*-spacing of 0.27 nm was bordered by MoP lattice fringes.[21] In selected yellow-dashed areas in Figure 1e, distorted basal planes were observed, indicating the lattice distortion of MoP introduced by the P/S substitution. Due to a similar *d*-spacing for the (100) plane of MoP and (100) plane of MoS_2, Fast Fourier transform (FFT) was performed to distinguish the two planes. As observed in Figure 1f, the corresponding FFT image exhibited a high crystalline structure indexed to MoS_2.[22-23] While in Figure 1g, the FFT pattern matched well with the hexagonal MoP phase.[24] The MoS_2 phase is interconnected with the MoP phase seamlessly, facilitating electron transfer across the interfaces, leading to an excellent catalytic performance. In addition, the difference in electronegativity between P and S prompts local charge density and yields the surface charge state.[25-26]

X-ray diffraction (XRD) profiles were collected to analyze the physical structure of the as-

prepared samples (Figure S4). The diffraction peaks at 27.9°, 32.2°, 43.1°, 64.9°, 67.0°, 67.8°, and 74.3° are ascribed to (001), (100), (101), (111), (200), (102), and (201) planes of the hexagonal MoP phase (JCPDS 24-0771).[10, 27-28] Noticeably, there are no S-related peaks observed from XRD, which can be explained by the low S-doping content. Raman spectroscopy was employed to analyze the MoS_2 phase in the composite. The MoO_3 peaks are absent from the Raman spectra, indicating a complete conversion of MoO_3 to MoP after CVD treatment. As presented in Figure S5a, E_{2g}^1 and A_{1g} modes are detected at 376 and 402 cm^{-1} in S-doped MoP samples. The E_{2g}^1 mode donates the opposite in-plane vibration of S atoms regarding to the Mo atom.[29] The A_{1g} mode is caused by out-of-plane vibration of S atoms in opposite directions.[30] With an increased CVD treatment duration, the intensities for E_{2g}^1 and A_{1g} modes also increase, indicating more MoS_2 phase in the composite. However, the full-width at half-maximum of E_{2g}^1 and A_{1g} modes increases with an increase in S content, which is probably due to structure deformation.[31] Moreover, both E_{2g}^1 and A_{1g} modes show a red-shift, revealing that structural changes may play a major role in altering atomic vibrations.[30] Raman mapping of the S-MoP NPL provides spatial intensity maps of the A_{1g} mode, as shown in Figure S5b, reflecting that S is uniformly distributed throughout the NPL. The chemical states were examined by X-ray photoelectron spectroscopy (XPS). Mo, P, and S were detected during the survey spectrum in Figure S6a, demonstrating that a S-doped MoP composite was obtained. The concentration of S can be tuned by adjusting the CVD treatment time. The S contents are estimated to be about 1.2 at%, 3.4 at%, and 6.3 at% in the S-doped MoP NPL at sulfuration times of 15 min, 30 min, 60 min, respectively. The chemical states were investigated by high-resolution XPS, as exhibited in Figure S6b-d. In the Mo 3d spectrum, peaks located 231.1 eV and 228.5 eV are indexed with Mo^{4+} in MoP, coinciding with previous reports.[32-35] The binding energy peaks located at 232.2

eV and 229.3 eV were indexed to Mo^{4+} $3d_{3/2}$ and Mo^{4+} $3d_{5/2}$ in MoS_2 phase.[36] In the P 2p profile, peaks at 129.6 eV and 130.5 eV are consistent with P^{4-} in MoP.[19, 32, 37] For the S 2s profile, peaks with binding energies of 161.8 eV and 163.1 eV are ascribed to S^{2-} in MoS_2 phase.[38-40] No peaks corresponding to the Mo-O were observed. (Note that the surface of S-MoP NPL is very easy to be oxidized, so the sample should be stored in the glove box or inert gas before testing.) The compilation of these results reveals that the S-doped MoP composite was successfully fabricated by a two-step CVD treatment.

To determine the optimal fabrication condition for MoP NPL, linear sweep voltammetry (LSV) was employed to evaluate the HER performance of various NPL samples (Figure S7) employing a homemade reactor in 0.5 M H_2SO_4 electrolyte (pH=0). It should be noted that iR-correction was performed for all LSV data. The MoP NPL fabricated by CVD treatment at 500 ^oC (MoP-500) exhibited the favorable electrocatalytic activities with an onset-overpotential (η_{onset}) of 89 mV and overpotential (η_{10}) of 117 mV at 10 mA cm^{-2}, which were lower than MoO_3 NPL and MoP NPL. Moreover, MoP-500 NPL presented the largest exchange current density of 0.21 mA cm^{-2}, about 3-4 times larger than that obtained from MoP-400 (annealed at 400 ^oC) and MoP-600 (annealed at 600 ^oC), revealing outstanding hydrogen evolution activity and fast charge transfer. Therefore, the following research was performed based on the MoP-500 NPL.

As illustrated in Figure 2a, 3.4 at% S-doped MoP (S-MoP in the following discussion denotes 3.4 at% S-doped MoP) NPL showed a prominent larger current density and lower onset-overpotential in the acidic electrolyte as compared to other S-doped MoP NPL with 1.2 at% and 6.3 at% doping contents. The S-MoP NPL requires 86 mV, 104 mV and 145 mV to deliver 10 mA cm^{-2}, 20 mA cm^{-2}, and 100 mA cm^{-2}, respectively, which is much lower than the state-of-the-art metal sulfides and metal phosphides HER catalysts (Table S1). As generally accepted,

HER mechanism can be ascribed to the following three possible pathways in the acidic electrolyte:[34]

(1) Volmer step: $H^+ + e^- \rightarrow H_{ads}$

(2) Heyrovsky step: $H_{ads} + H^+ + e^- \rightarrow H_2$

(3) Tafel step: $2H_{ads} \rightarrow H_2$

where H_{ads} donates an adsorbed hydrogen atom on the catalyst surface. Therefore, H_2 can be generated via Volmer-Heyrovsky reaction or the Volmer-Tafel reaction.

The Tafel slope of S-MoP NPL was computed to 34 mV dec^{-1}, which can be comparable to the Tafel slope for a Pt/C catalyst (30 mV dec^{-1}) and much lower than those of 79 mV dec^{-1} for 1.2 at% S-MoP NPL and 62 mV dec^{-1} for 6.3 at% S-MoP NPL, as shown in Figure 2b.[39] A lower Tafel slope indicates better electron transfer within the S-doped MoP NPL. The Tafel slope obtained here suggests that a Volmer-Tafel reaction occurs in the S-MoP NPL and that the Tafel step is rate-determining during the HER process. While a typical Volmer-step-determined, the Volmer-Heyrovsky reaction route was revealed for 1.2 at% and 6.3 at% S-MoP NPL.[36-37] Moreover, the exchange current densities (j_0) were calculated to be 0.35, 0.76, and 0.21 mA cm^{-2}, presenting excellent intrinsic catalytic activities of the as-prepared S-MoP NPL under equilibrium conditions. The S-MoP NPL exhibits higher exchange current density (0.76 mA cm^{-2}) and lower overpotential/Tafel slope (34 mV dec^{-1}), which contributes to superior catalytic activity (for details see Table S1).

To develop a pH-universal catalytic electrode, the HER activities of MoP and S-MoP NPL were evaluated in 1.0 M KOH electrolyte (pH=14). Figure 2c illustrates the LSV curves after iR-correction. As shown in Figure S8, S-MoP NPL shows much higher cathodic current densities and lower overpotentials, exhibiting very good HER activity in a basic electrolyte (more details

see Table S2). The S-MoP NPL required 104 mV to deliver 10 mA cm^{-2} in 1.0 M KOH electrolyte, while 182 mV was needed for pristine MoP NPL to deliver 10 mA cm^{-2}. The S-MoP NPL presents Tafel slopes of 56 mV dec^{-1} in Figure 2d, which is smaller than that of pristine MoP (178 mV dec^{-1}) in KOH electrolyte. Moreover, the catalytic behavior in 1.0 M PBS solution (pH=7) was assessed, as shown in Figure 2c. The S-MoP NPL presents a lower cathodic current density than those in 0.5 M H_2SO_4 and 1.0 M KOH electrolyte, but still higher than that of pristine MoP NPL. The double-layer capacitance in Figure S9 reveals the large electrochemically active surface area (EASA) for the S-MoP, indicating more active sites for HER were exposed after S doping.

Additionally, the S-MoP NPL requires 142 mV to drive 10 mA cm^{-2}, which is much lower than most other catalysts in PBS solution (more details see Table S3). Tafel slopes of S-MoP NPL and MoP NPL derived from LSV curves were computed to 98 and 205 mV dec^{-1}, respectively.

The HER mechanisms under basic and neutral conditions are ambiguous, however, Durst et al. have suggested that Volmer and Heyrovsky steps do not change in accordance with changes in pH. Although it is difficult to judge the rate-determining steps in basic and neutral electrolytes, the establishment of Tafel slopes can elucidate important information. Tafel slopes for S-MoP NPL increased from 34 mV dec^{-1} in 0.5 M H_2SO_4 electrolyte to 106 and 148 mV dec^{-1} in 1 M KOH and 1 M PBS solutions, respectively, due to the considerably lower proton concentration.[35] Therefore, the S-MoP NPL in basic and neutral electrolytes still revealed a Volmer-Heyrovsky reaction and the Volmer step is rate-determining.

The long-term electrochemical behavior toward HER (Figure 2e) was conducted in acidic (pH=0), basic (pH=14) and neutral (pH=7) electrolytes, where the S-MoP NPL maintained

stabilities at 10 mA cm^{-2} for 30,000 seconds. As displayed in Figure S10, surface morphology is preserved after long-term electrochemical stability testing, demonstrating that the stability of the binder-free thin-film catalyst can be a significant alternative to powder catalysts. Moreover, the cross-sectional SEM of the S-MoP NPL, as shown in Figure S11, was performed after long-term testing in 0.5 M H_2SO_4. It is observed that the thickness and the morphology are consistent with those before testing, indicating the excellent stability after testing.

Transition metal M-edge spectroscopy is a materials characterization tool, using soft X-ray photons to investigate 3p-3d or 3p-4d transition.[38] Due to Coulomb and exchange coupling between 3d or 4d electrons and 3p core holes, the M-edge line shape can reflect oxidation state, ligand field and spin state of the examined transition metal.[39] Figure 3a shows the Mo M_3-edge X-ray absorption spectroscopy (XAS) that represents the transitions from a $3p^6 4d^0$ ground state to a $3p^5 4d^1$ excited state. The well-resolved two main peaks of MoP account for the electronic spin-orbital L-S interactions between the ground and final state, which is very similar to the spectrum observed in MoO_4^{2-}.[43] Interestingly, only one dominant peak is observed for S-doped MoP, and the spectrum is in consistency with that of MoS_4^{2-},[40] suggesting the successful doping of S. With the formation of Mo-S bonding, the $Mo^{4+}(4d^2)$ formation locates at the top of the S^{2-} ($3p^6$) band. The Mo-Mo 4d electron bonding is constituted as zigzag chains, which permits Mo-Mo bonding with the three t_2 orbitals,[41] as demonstrated by a molecular orbital study.[42] These features different from MoP make the p-d electron transition an interatomic-like transition of a d-d band, delocalizing in the Mo 4d state but not to an atomic-like transition as that of MoO_4^{2-} and MoP,[41] which results in one major peak in the spectrum. Note that S-doped MoP has a lower M_3-edge XAS peak and broader spectrum compared to MoP. A previous study has shown B-doped $MoSe_2$ can induce strong hybridization among Mo 3d, Se 2p, and B 2p orbitals,[43] thus creating

more gap states at the Fermi level, which could be responsible for the broader spectrum in S-doped MoP in our case. In addition, the band alignment using XAS, X-ray emission and XPS indicates the stronger hybridization leads to a smaller band gap.[44] This suggests that S-doped MoP could have a smaller band gap that can increase the electrical conductivity and facilitate electron movement and charge transfer. This is consistent with previous works for B-doped $MoSe_2$ and surface modified MoS_2.[43, 45] To confirm the S chemistry in S-doped MoP, the S K-edge X-ray absorption near edge structure (XANES) measurements were conducted at beamline 9-BM of the Advanced Photon Source. Due to the low concentration of S, the XANES spectra have a high noise level. As shown in Figure 3b and c, the S XANES of S-doped MoP is similar to that of MoS_2, suggesting the same oxidation state as MoS_2. This similarity can be better seen from the derivative of S XANES, which is more reliable for oxidization state. S XAS results are consistent with the XPS results and also support Mo M-edge XAS. The Mo K-edge and L-edge XAS (Figure S12) were also measured to check the change of Mo oxidization state and local structure. However, due to the thick Mo substrate and the bulk-sensitivity of the high energy hard X-ray compared to soft X-ray, the Mo metal information is dominant.

The equilibrium structures of 2D layer MoS_2, MoP, and S-doped MoP are obtained by the B3LYP-D2 method and shown in Figure 3d-f, respectively. The electronic properties were computed at the equilibrium geometries. The present study found that the monolayer MoS_2 and MoP have a direct band gap about ~2.18 eV and ~2.07 eV, respectively; see Figure 3g-i. When S-atoms were doped in the pristine MoP i.e. S-MoP, the electronic band gap became about 0.62 eV, thus S-doping was able to decrease the band gap as described in the band structures and DOSs computations, presenting in Figure 3i. In other words, this result not only supports the Mo M-edge XAS but also indicates that S-MoP is going to have low direct band gap ~0.62 eV

compared to the pristine material, which shows that S-doping is useful for HER. Thus, the S-doping influences the electronic properties of the pristine and S-doped MoP in this work. The addition of S atoms doped in MoP rectifies the electron accumulation in the conduction and valence bands as depicted in the DOSs implying high electron mobility. Thus, we can say that S-doped MoP is a better catalyst for HER compared to pristine MoS_2 and MoP, owing to their intrinsic electronic properties as well.

In order to model the surfaces of MoS_2, MoP, and S-doped MoP, we used cluster models following the approach employed in recent computational studies (Figure S13).[46, 47] The cluster models for MoS_2, MoP, and S-doped MoP are named here as MoS′, MoP′, and 5%-MoPS′ or 10%-MoPS′, respectively. In the MoP′ and MoPS′ models, H atoms saturate the dangling bonds of P along the edges. We studied several possible configurations of 10%-MoPS′ to find most efficient HER catalyst (Figure S13). Although the cluster models used here may not capture all effects of porous MoP and MoPS layers, they are useful to understand the energetics of HER mechanisms over edge atoms of the catalyst and the effects due to different S contents. Our current experimental results and previous computational studies indicate Volmer-Heyrovski mechanism as the preferred pathways for HER over MoS_2, MoP and S-doped MoP materials.[46, 47] Therefore, we studied the kinetics and thermodynamics for these steps over MoS_2, MoP, and S-doped MoP systems. The HER reaction is initiated by the absorption of a hydride ion on energetically favorable S (or P) site. This follows a hydride shift to the reactive, neighboring metal (Mo) site (Figure S14). Subsequently, the H_2 formation would occur preferentially over the Mo site via the reaction of a Mo-absorbed hydride ion with a solvated proton (modeled here as $H_9O_4^+$) from the solution. Recent studies have predicted that for 1T MoS_2, the H_2 formation can occur over S site without the need of an initial H transfer.[48, 49] However, this process is

energetically unfavorable for 2H MoS_2 modeled in the current study. The H_2 formation step (also known as the Heyrovsky mechanism) has been identified to be the rate-determining process for reactions over MoS_2. A rationale for modeling these processes may be found elsewhere.[46, 47] Our calculations show that the hydride migration from S to Mo over MoS′ is facile due to the presence of a small activation barrier ($\Delta G^{\ddagger}$ = 4.5 kcal/mol) and a large exergonicity (ΔG = -23.6 kcal/mol). This step is favorable when the whole system is negatively charged than when it is neutral or positively charged. When MoP′ is used as the catalyst, this step becomes unfavorable ($\Delta G^{\ddagger}$ = 17.5 kcal/mol and ΔG = 9.9 kcal/mol) and the rate-determining process. Interestingly, the Heyrovski step occurs more rapidly over MoP′ than MoS′. Calculated free energy barrier ($\Delta G^{\ddagger}$) and reaction free energy (ΔG) are favored over MoP′ than over MoS′ by 7.1 and 1.8 kcal/mol, respectively.

To understand the effects of S-doping, we studied the rate-determining Volmer step over 5% and 10% S-doped MoPS systems. Calculations predict a smaller activation free energy of 12.9 kcal/mol for HER over 5%-MoPS′ compared to 17.5 kcal/mol required over MoP′ (Figure 4), which is associated with the experimental findings. Similarly, a more favorable activation free energy is revealed for 5% S-doped system. When the percentage of S-doping increased to 10%, both activation free energy and reaction endergonicity are increased. These results strongly suggest that small S-doping could accelerate HER over MoPS′. Among different configurations studied for 10%-MoPS′, the one with S-M-S bond along the edge is more HER active than other systems. This suggests that HER might preferentially occur on the edges along the boundaries of MoS_2 and MoP phases. However, more calculations would be required to confirm this prediction, which is beyond the scope of the present work. We also studied different mechanisms, where H absorbed initially on P migrating to Mo site via an intermediate absorption over S sites. However,

this step requires higher activation free energy and hence discarded. To summarize, our calculations of HER mechanisms confirm higher activity found for S-doped MoP with small S concentration and explains experimentally observed reactivity trends.

The superior HER activity of S-MoP NPL at pH-universal electrolyte can be explained as follows: 1) S-MoP NPL can be employed as a binder-free electrode for HER, minimizing the electrode resistance and facilitating electron/ion diffusion. (2) The porous morphology promotes proton transport and hydrogen adsorption, therefore enhancing electron transfer efficiently. S-MoP NPL exhibits a higher electrochemically active surface area, owing to the boundaries between MoP and MoS_2 could act as catalytically active sites to improve electrochemical performance. (3) The presence of S-dopant decreases the free energy for Volmer step during the HER reactions. The S-MoP NPL exhibits the free energy of hydrogen adsorption is approximately zero, which facilitates the hydrogen atom adsorbed on the surface of the catalyst. Additionally, S-MoP NPL presents with minimum hydrogen binding energy above the valence band maximum, making it easier to accept electrons from adsorbed hydrogen atoms.

CONCLUSION

In summary, a self-organized S-doped MoP NPL was successfully prepared through anodization and a two-step CVD treatment process. As a versatile electrocatalytic electrode for HER, the S-MoP NPL presented an excellent catalytic performance in all pH-universal electrolytes. The addition of S atoms doped in MoP rectifies the electron accumulation in the conduction and valence bands implying high electron mobility. Calculations using cluster models indicate that the HER reactions over MoPS with a small percentage of S-doping are more favorable as compared to that over MoS_2, MoP, and MoPS with larger S-doping. This work not only provides a versatile and high-activity electrode for hydrogen fuel generation but also

provides a better understanding of the synergic effects on electrochemical reactions.

Corresponding Author

*****Correspondence and requests for materials should be addressed to Y.Y. (Yang.Yang@ucf.edu) J.L.M.C. (mendoza@eng.famu.fsu.edu) or Z. F. (zhenxing.feng@oregonstate.edu).

Author Contributions

Y.Y. and K.L. designed the experiments. K.L. and K.M. performed the materials synthesis and characterization. M. W., G. E. S., and Z. F. conducted the X-ray absorption measurements. Z.Y. performed the STEM/EELS analysis under the direction of Y.D. J.L.M.-C., S.P., A.N, and C.I.A.-V. designed, executed and analyzed the simulations and the theoretical calculations. A.N performed all cluster model calculations of HER mechanisms, analyzed and wrote the results. Y.Y., J.L.M.C, Z. F. A. N. and K.L. wrote the manuscript. Y.Y. and J.L.M.C corrected the manuscript. K.L. & S.P. contributed equally to this paper. All authors approved the manuscript.

Notes

The authors declare no competing financial interest.

ACKNOWLEDGEMENTS

This work was financially supported by the University of Central Florida through a start-up grant (No. 20080741). The authors greatly thank Dr. Yong-Ho Sohn and Dr. Nina Orlovskaya for Characterization help in TEM and Raman. Y.D. acknowledges support from the US Department of Energy, Office of Science, Office of Basic Energy Sciences, Early Career Research Program for the TEM work performed at the William R. Wiley Environmental Molecular Sciences Laboratory, a national user facility sponsored by US Department of Energy, Office of Biological and Environmental Research and located at PNNL. J.L.M.C. acknowledges the start-up funds from Florida State University and the Energy and Material Initiative. J.L.M.-C., S.P., N.A., and

C.I.A.-V. acknowledge the HPC cluster at the Research Computing Center (RCC) of Florida State University and facilities at the High-Performance Material Institute. A portion of this work was performed at the National High Magnetic Field Laboratory, which is supported by National Science Foundation Cooperative Agreement No. DMR-1644779 and the State of Florida. Z. F. thanks the technical support from Alpha N'Diaye at Advanced Light Source (ALS) and Qing Ma at Advanced Photon Source (APS), and the Callahan Faculty Scholar Endowment Fund from Oregon State University. The ALS is an Office of Science User Facility operated for the U.S. Department of Energy (DOE) Office of Science by Lawrence Berkeley National Laboratory and supported by the DOE under Contract No. DEAC02-05CH11231. Use of the APS, an Office of Science User Facility operated for the U.S. Department of Energy (DOE) Office of Science by Argonne National Laboratory, was supported by the U.S. DOE under Contract no. DE-AC02-06CH11357.

Supporting Information

Experimental details, SEM/TEM images, XRD/Raman/XPS data, and HER performance tables are available free of charge on the ACS Publication website.

REFERENCES

1. Zheng, Y.; Jiao, Y.; Zhu, Y.; Li, L. H.; Han, Y.; Chen, Y.; Du, A.; Jaroniec, M.; Qiao, S. Z., Hydrogen Evolution by a Metal-Free Electrocatalyst. *Nat. Commun.* **2014,** *5*, 3783.

2. Liang, K.; Tang, X.; Hu, W., High-Performance Three-Dimensional Nanoporous NiO Film as a Supercapacitor Electrode. *J. Mater. Chem.* **2012,** *22* (22), 11062-11067.

3. Liang, K.; Marcus, K.; Zhang, S.; Zhou, L.; Li, Y.; De Oliveira, S. T.; Orlovskaya, N.; Sohn, Y. H.; Yang, Y., NiS_2/FeS Holey Film as Freestanding Electrode for High-Performance

Lithium Battery. *Adv. Energy Mater.* **2017,** *7*, 1701309.

4. Liang, K.; Marcus, K.; Guo, L.; Li, Z.; Zhou, L.; Li, Y.; De Oliveira, S. T.; Orlovskaya, N.; Sohn, Y. H.; Yang, Y., Freestanding NiS_x Porous Film as Binder-Free Electrode for Mg-Ion Battery. *Chem. Commun.* **2017,** *53*, 7608-7611.

5. Liang, K.; Yan, Y.; Guo, L.; Marcus, K.; Li, Z.; Zhou, L.; Li, Y.; Ye, R.; Orlovskaya, N.; Sohn, Y. H., Yang, Y., Strained $W(Se_xS_{1-x})_2$ Nanoporous Films for High Efficient Hydrogen Evolution. *ACS Energy Lett.* **2017,** *2*, 1315-1320.

6. Liu, P.; Rodriguez, J. A., Catalysts for Hydrogen Evolution from the [NiFe] Hydrogenase to the Ni_2P (001) Surface: the Importance of Ensemble Effect. *J. Am. Chem. Soc.* **2005,** *127* (42), 14871-14878.

7. Prins, R.; Bussell, M. E., Metal Phosphides: Preparation, Characterization and Catalytic Reactivity. *Catal. Lett.*, **2012,** *142* (12), 1413-1436.

8. Bai, J.; Li, X.; Wang, A.; Prins, R.; Wang, Y., Different Role of H_2S and Dibenzothiophene in the Incorporation of Sulfur in the Surface of Bulk MoP During Hydrodesulfurization. *J. Catal.* **2013,** *300*, 197-200.

9. Zhang, Z.; Hao, J.; Yang, W.; Lu, B.; Tang, J., Modifying Candle Soot with FeP Nanoparticles into High-Performance and Cost-Effective Catalysts for the Electrocatalytic Hydrogen Evolution Reaction. *Nanoscale* **2015,** *7* (10), 4400-4405.

10. Kibsgaard, J.; Jaramillo, T. F., Molybdenum Phosphosulfide: An Active, Acid-Stable, Earth-Abundant Catalyst for the Hydrogen Evolution Reaction. *Angew. Chem. Int. Ed.* **2014,** *53* (52), 14433-14437.

11. Ye, R.; del Angel-Vicente, P.; Liu, Y.; Arellano-Jimenez, M. J.; Peng, Z.; Wang, T.; Li, Y.; Yakobson, B. I.; Wei, S. H.; Yacaman, M. J., High-Performance Hydrogen Evolution from

$MoS_{2(1-x)}P_x$ Solid Solution. *Adv. Mater.* **2016,** *28* (7), 1427-1432.

12. Wu, A.; Tian, C.; Yan, H.; Jiao, Y.; Yan, Q.; Yang, G.; Fu, H., Hierarchical MoS_2@ MoP Core–Shell Heterojunction Electrocatalysts for Efficient Hydrogen Evolution Reaction over a Broad pH Range. *Nanoscale* **2016,** *8* (21), 11052-11059.

13. Zou, X.; Huang, X.; Goswami, A.; Silva, R.; Sathe, B. R.; Mikmekova, E.; Asefa, T., Cobalt-Embedded Nitrogen-Rich Carbon Nanotubes Efficiently Catalyze Hydrogen Evolution Reaction at all pH Values. *Angew. Chem.* **2014,** *126* (17), 4461-4465.

14. Gao, S.; Li, G.-D.; Liu, Y.; Chen, H.; Feng, L.-L.; Wang, Y.; Yang, M.; Wang, D.; Wang, S.; Zou, X., Electrocatalytic H_2 Production from Seawater over Co, N-Codoped Nanocarbons. *Nanoscale* **2015,** *7* (6), 2306-2316.

15. Cheon, J. Y.; Kim, J. H.; Kim, J. H.; Goddeti, K. C.; Park, J. Y.; Joo, S. H., Intrinsic Relationship between Enhanced Oxygen Reduction Reaction Activity and Nanoscale Work Function of Doped Carbons. *J. Am. Chem. Soc.* **2014,** *136* (25), 8875-8878.

16. Liang, K.; Guo, L.; Marcus, K.; Zhang, S.-F.; Yang, Z.; Perea, D. E.; Zhou, L.; Du, Y.; Yang, Y., Overall Water Splitting Using Room-Temperature Synthesized NiFe Oxyfluoride Nanoporous Films. *ACS Catal.* **2017,** *7*, 8406-8412.

17. Liang, K.; Li, L.; Yang, Y., Inorganic Porous Films for Renewable Energy Storage. *ACS Energy Lett.* **2017,** *2* (2), 373-390.

18. Guo, L.; Liang, K.; Marcus, K.; Li, Z.; Zhou, L.; Mani, P. D.; Chen, H.; Shen, C.; Dong, Y.; Zhai, L.; Coffey, K.; Orlovskaya, N.; Sohn, Y. H.; Yang, Y., Enhanced Photoelectrocatalytic Reduction of Oxygen Using Au@TiO_2 Plasmonic Film. *ACS Appl. Mater. Interfaces* **2016,** *8* (51), 34970-34977.

19. Xiao, P.; Sk, M. A.; Thia, L.; Ge, X.; Lim, R. J.; Wang, J.-Y.; Lim, K. H.; Wang, X.,

Molybdenum Phosphide as an Efficient Electrocatalyst for the Hydrogen Evolution Reaction. *Energy Environ. Sci.* **2014,** *7* (8), 2624-2629.

20. Sun, A.; Shen, Y.; Wu, Z.; Wang, D., N-doped MoP Nanoparticles for Improved Hydrogen Evolution. *Int. J. Hydro.Energy* **2017,** *42* (21), 14566-14571.

21. Hansen, L. P.; Ramasse, Q. M.; Kisielowski, C.; Brorson, M.; Johnson, E.; Topsøe, H.; Helveg, S., Atomic-Scale Edge Structures on Industrial-Style MoS_2 Nanocatalysts. *Angew. Chem. Int. Ed.* **2011,** *50* (43), 10153-10156.

22. Hussain, S.; Singh, J.; Vikraman, D.; Singh, A. K.; Iqbal, M. Z.; Khan, M. F.; Kumar, P.; Choi, D.-C.; Song, W.; An, K.-S., Large-Area, Continuous and High Electrical Performances of Bilayer to Few Layers MoS_2 Fabricated by RF Sputtering via Post-Deposition Annealing Method. *Sci. Rep.* **2016,** *6,* 30791.

23. Gao, D.; Si, M.; Li, J.; Zhang, J.; Zhang, Z.; Yang, Z.; Xue, D., Ferromagnetism in Freestanding MoS_2 Nanosheets. *Nanoscale Res. Lett.* **2013,** *8* (1), 129.

24. Chen, Z.; Lv, C.; Chen, Z.; Jin, L.; Wang, J.; Huang, Z., Molybdenum Phosphide Flakes Catalyze Hydrogen Generation in Acidic and Basic Solutions. *Am. J. Analy. Chem.* **2014,** *5* (17), 1200.

25. Xiao, P.; Chen, W.; Wang, X., A Review of Phosphide-Based Materials for Electrocatalytic Hydrogen Evolution. *Adv. Energy Mater.* **2015,** *5* (24), 1500985.

26. Yan, H.; Tian, C.; Wang, L.; Wu, A.; Meng, M.; Zhao, L.; Fu, H., Phosphorus-Modified Tungsten Nitride/Reduced Graphene Oxide as a High-Performance, Non-Noble-Metal Electrocatalyst for the Hydrogen Evolution Reaction. *Angew. Chem. Int. Ed.* **2015,** *54* (21), 6325-6329.

27. Deng, C.; Ding, F.; Li, X.; Guo, Y.; Ni, W.; Yan, H.; Sun, K.; Yan, Y.-M., Templated-

Preparation of a Three-Dimensional Molybdenum Phosphide Sponge as a High Performance Electrode for Hydrogen Evolution. *J. Mater. Chem. A* **2016,** *4* (1), 59-66.

28. Jia, J.; Zhou, W.; Li, G.; Yang, L.; Wei, Z.; Cao, L.; Wu, Y.; Zhou, K.; Chen, S., Regulated Synthesis of Mo Sheets and Their Derivative MoX Sheets (X: P, S, or C) as Efficient Electrocatalysts for Hydrogen Evolution Reactions. *ACS Appl. Mater. Interfaces* **2017,** *9* (9), 8041-8046.

29. Shi, Y.; Zhou, Y.; Yang, D.-R.; Xu, W.-X.; Wang, C.; Wang, F.-B.; Xu, J.-J.; Xia, X.-H.; Chen, H.-Y., Energy Level Engineering of MoS_2 by Transition-Metal Doping for Accelerating Hydrogen Evolution Reaction. *J. Am. Chem. Soc.* **2017**, *139* (43), 15479-15485.

30. Li, H.; Zhang, Q.; Yap, C. C. R.; Tay, B. K.; Edwin, T. H. T.; Olivier, A.; Baillargeat, D., From Bulk to Monolayer MoS_2: Evolution of Raman Scattering. *Adv. Funct. Mater.* **2012,** *22* (7), 1385-1390.

31. Yan, Y.; Li, F.; Gong, Y.; Yao, M.; Huang, X.; Fu, X.; Han, B.; Zhou, Q.; Cui, T., Interlayer Coupling Affected Structural Stability in Ultrathin MoS_2: An Investigation by High Pressure Raman Spectroscopy. *J. Phys. Chem. C* **2016,** *120* (43), 24992-24998.

32. Yao, Z.; Su, Y.; Lu, C.; Yang, C.; Xu, Z.; Zhu, J.; Zhuang, X.; Zhang, F., Template-Directed Approach to Two-Dimensional Molybdenum Phosphide-Carbon Nanocomposites with High Catalytic Activities in the Hydrogen Evolution Reaction. *New J. Chem.* **2016,** *40* (7), 6015-6021.

33. Xing, Z.; Liu, Q.; Asiri, A. M.; Sun, X., Closely Interconnected Network of Molybdenum Phosphide Nanoparticles: a Highly Efficient Electrocatalyst for Generating Hydrogen from Water. *Adv. Mater.* **2014,** *26* (32), 5702-5707.

34. Bai, J.; Li, X.; Wang, A.; Prins, R.; Wang, Y., Hydrodesulfurization of Dibenzothiophene

and its Hydrogenated Intermediates over Bulk MoP. *J. Catal.* **2012,** *287*, 161-169.

35. Jia, J.; Xiong, T.; Zhao, L.; Wang, F.; Liu, H.; Hu, R.; Zhou, J.; Zhou, W.; Chen, S., Ultrathin N-doped Mo_2C Nanosheets with Exposed Active Sites as Efficient Electrocatalyst for Hydrogen Evolution Reactions. *ACS Nano* **2017,** *11* (12), 12509-12518.

36. Da Silveira Firmiano, E. G.; Rabelo, A. C.; Dalmaschio, C. J.; Pinheiro, A. N.; Pereira, E. C.; Schreiner, W. H.; Leite, E. R., Supercapacitor Electrodes Obtained by Directly Bonding 2D MoS_2 on Reduced Graphene Oxide. *Adv. Energy Mater.* **2014,** *4* (6), 1301380.

37. Li, G.; Yu, J.; Jia, J.; Yang, L.; Zhao, L.; Zhou, W.; Liu, H., Cobalt–Cobalt Phosphide Nanoparticles@ Nitrogen - Phosphorus Doped Carbon/Graphene Derived from Cobalt Ions Adsorbed Saccharomycete Yeasts as an Efficient, Stable, and Large - Current - Density Electrode for Hydrogen Evolution Reactions. *Adv. Funct. Mater.* **2018**, *28* (40), 1801332.

38. Hu, Y., and Chua, D. H., Synthesizing 2D MoS_2 Nanofins on Carbon Nanospheres as Catalyst Support for Proton Exchange Membrane Fuel Cells. *Sci. Rep.* **2016,** 6, 28088.

39. Gao, M.-R.; Liang, J.-X.; Zheng, Y.-R.; Xu, Y.-F.; Jiang, J.; Gao, Q.; Li, J.; Yu, S.-H., An Efficient Molybdenum Disulfide/Cobalt Diselenide Hybrid Catalyst for Electrochemical Hydrogen Generation. *Nat. Commun.* **2015,** *6,* 5982.

40. Yang, L.; Zhou, W.; Lu, J.; Hou, D.; Ke, Y.; Li, G.; Tang, Z.; Kang, X.; Chen, S., Hierarchical Spheres Constructed by Defect-Rich MoS_2/Carbon Nanosheets for Efficient Electrocatalytic Hydrogen Evolution. *Nano Energy* **2016,** *22*, 490-498.

41. Aritani, H.; Tanaka, T.; Funabiki, T.; Yoshida, S.; Eda, K.; Sotani, N.; Kudo, M.; Hasegawa, S., Study of the Local Structure of Molybdenum-Magnesium Binary Oxides by Means of Mo L3-edge XANES and UV-Vis Spectroscopy. *J. Phys. Chem.* **1996,** *100* (50), 19495-19501.

42. Hughbanks, T.; Hoffmann, R., Molybdenum Chalcogenides: Clusters, Chains, and Extended Solids. The Approach to Bonding in Three Dimensions. *J. Am. Chem. Soc.* **1983,** *105* (5), 1150-1162.

43. Gao, D.; Xia, B.; Zhu, C.; Du, Y.; Xi, P.; Xue, D.; Ding, J.; Wang, J., Activation of the $MoSe_2$ Basal Plane and Se-Edge by B Doping for Enhanced Hydrogen Evolution. *J. Mater. Chem. A* **2018,** *6* (2), 510-515.

44. Hong, W. T.; Stoerzinger, K. A.; Moritz, B.; Devereaux, T. P.; Yang, W.; Shao-Horn, Y., Probing $LaMO_3$ Metal and Oxygen Partial Density of States Using X-ray Dmission, Absorption, and Photoelectron Spectroscopy. *J. Phys. Chem. C* **2015,** *119* (4), 2063-2072.

45. Kim, Y.; Jackson, D. H.; Lee, D.; Choi, M.; Kim, T. W.; Jeong, S. Y.; Chae, H. J.; Kim, H. W.; Park, N.; Chang, H., In Situ Electrochemical Activation of Atomic Layer Deposition Coated MoS_2 Basal Planes for Efficient Hydrogen Evolution Reaction. *Adv. Funct. Mater.* **2017,** *27* (34), 1701825.

46. Lei, Y.; Pakhira, S.; Fujisawa, K.; Wang, X.; Iyiola, O. O.; Perea López, N. S.; Laura Elías, A.; Rajukumar, L. P.; Zhou, C.; Kabius, B., Low-Temperature Synthesis of Heterostructures of Transition Metal Dichalcogenide Alloys ($W_xMo_{1-x}S_2$) and Graphene with Superior Catalytic Performance for Hydrogen Evolution. *ACS Nano* **2017,** *11* (5), 5103-5112.

47. Huang, Y.; Nielsen, R. J.; Goddard, W. A.; Soriaga, M. P. The Reaction Mechanism with Free Energy Barriers for Electrochemical Dihydrogen Evolution on MoS_2. *J. Am. Chem. Soc.* **2015**, *137* (20), 6692–6698.

48. Tang, Q.; Jiang, D., Mechanism of Hydrogen Evolution Reaction on 1T-MoS_2 from First Principles. *ACS Catal*. **2016**, *6* (8), 4953-4961.

49. Chen, S.; Chen, X.; Wang, G.; Liu, L.; He, Q.; Li, X.; Cui, N., Reaction Mechanism with

Thermodynamic Structural Screening for Electrochemical Hydrogen Evolution on Monolayer 1T' Phase MoS_2. *Chem. Mater.* 2018, 30 (15), 5404-5411.

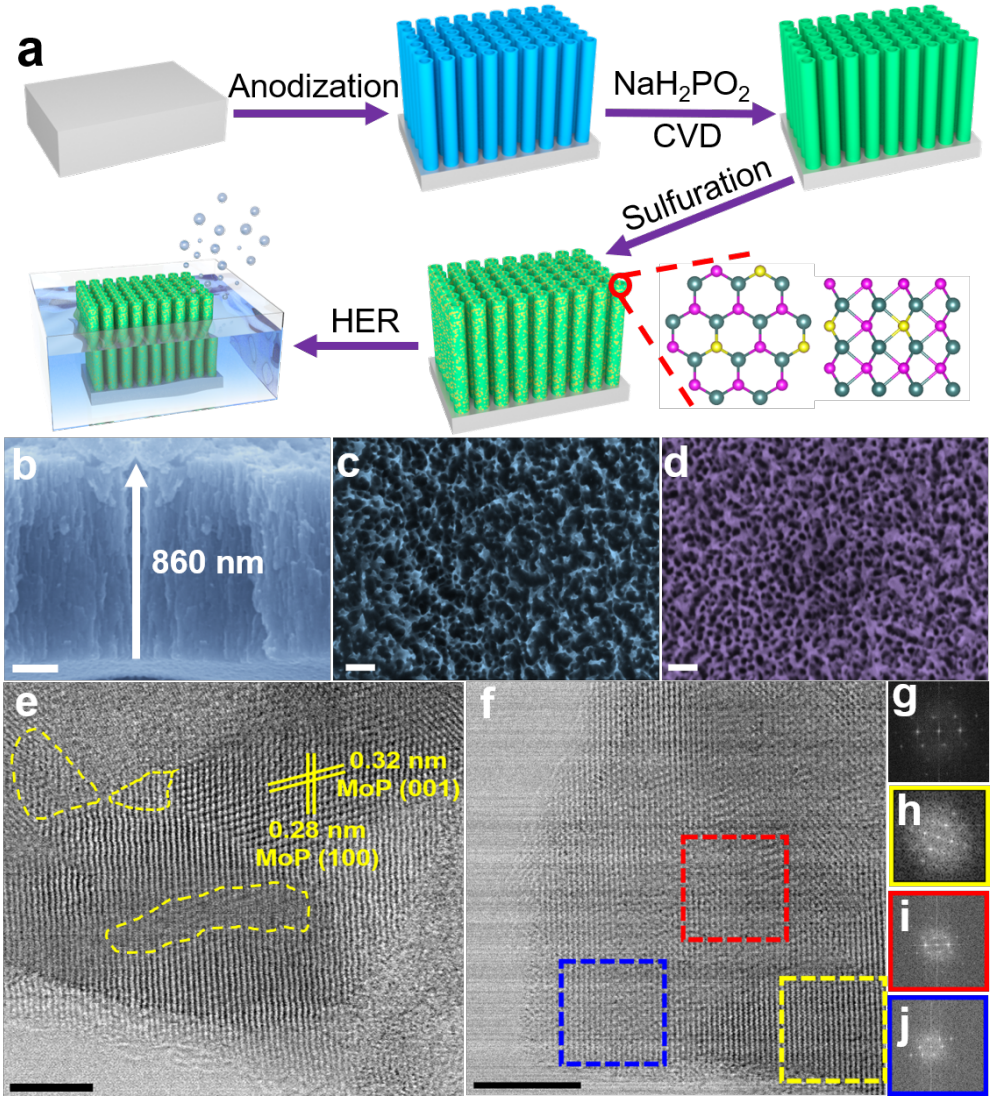

Figure 1. Schematic illustration of the synthesis process and morphological characterization. (a) Schematic illustration outlining S-doped MoP nanoporous layer (NPL) fabrication. The green, red and yellow balls denote Mo, P, and S, respectively. (b) Cross-sectional SEM image of NPL after anodization. (c-d) Top-view SEM images of MoP-500 and 3.4 at% S-MoP NPL, respectively. (e-f) HRTEM image of 3.4 at% S-MoP NPL. Yellow-dashed areas donate distorted basal planes. (g-j) Fast Fourier transform (FFT) was conducted on (f) and selected area, respectively. The scale bars in (b-d), (e) and (f) donate 200 nm, 2 nm, and 5nm, respectively.

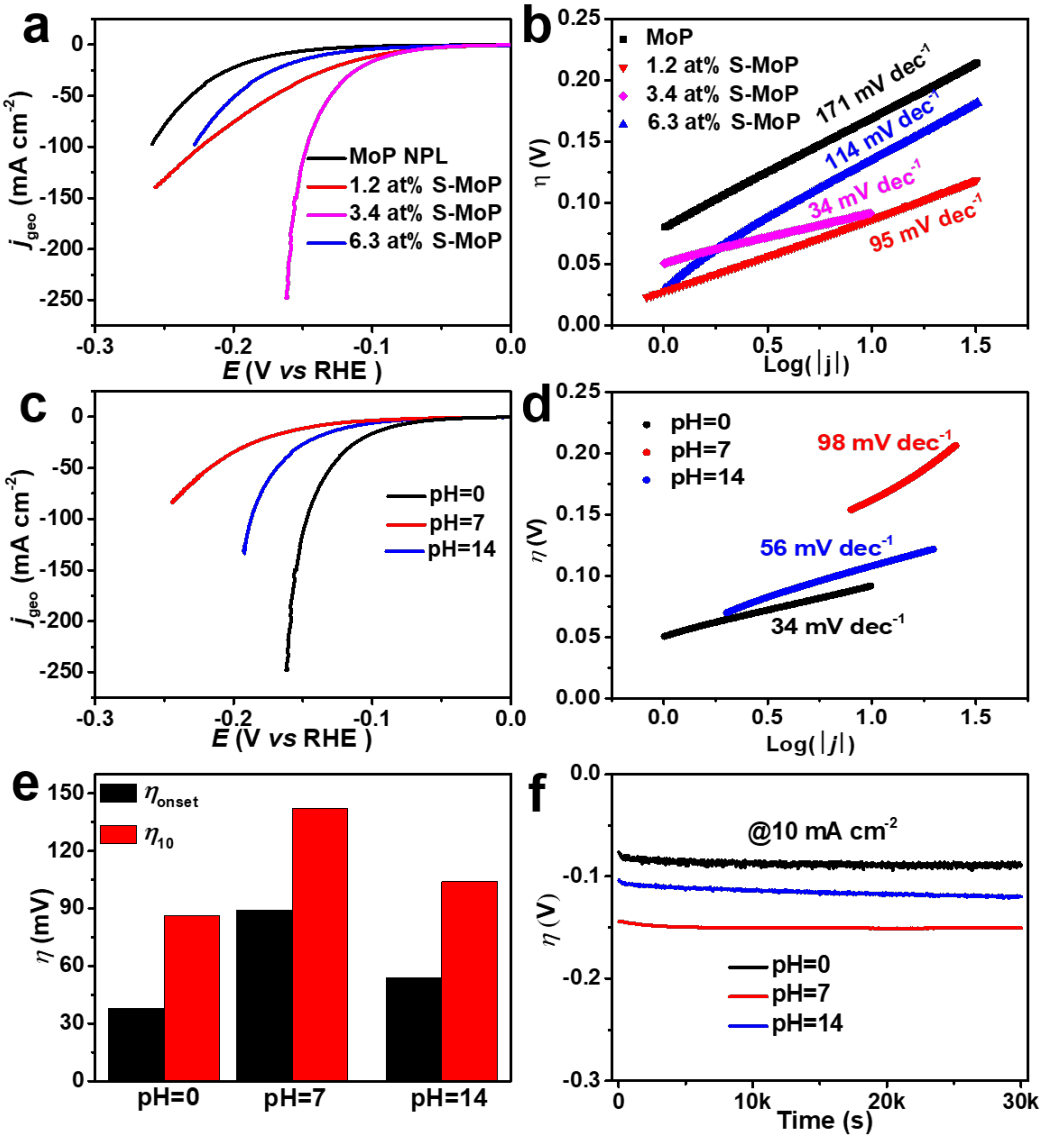

Figure 2. Electrochemical performance of NPL. (a-b) iR-corrected polarized curves for HER measured at 5 mV s^{-1} and corresponding Tafel slope in 0.5 M H_2SO_4 electrolyte. (c-d) iR-corrected LSV curves measured at 5 mV s^{-1} and corresponding Tafel slope in 0.5 M H_2SO_4, 1.0 M KOH, and 1.0 M PBS aqueous solution, respectively. (e) Overpotential and Tafel slope of 3.4 at% S-MoP NPL. (f) The long-term electrochemical stabilities of HER with a constant current density of 10 mA cm^{-2} in different electrolytes.

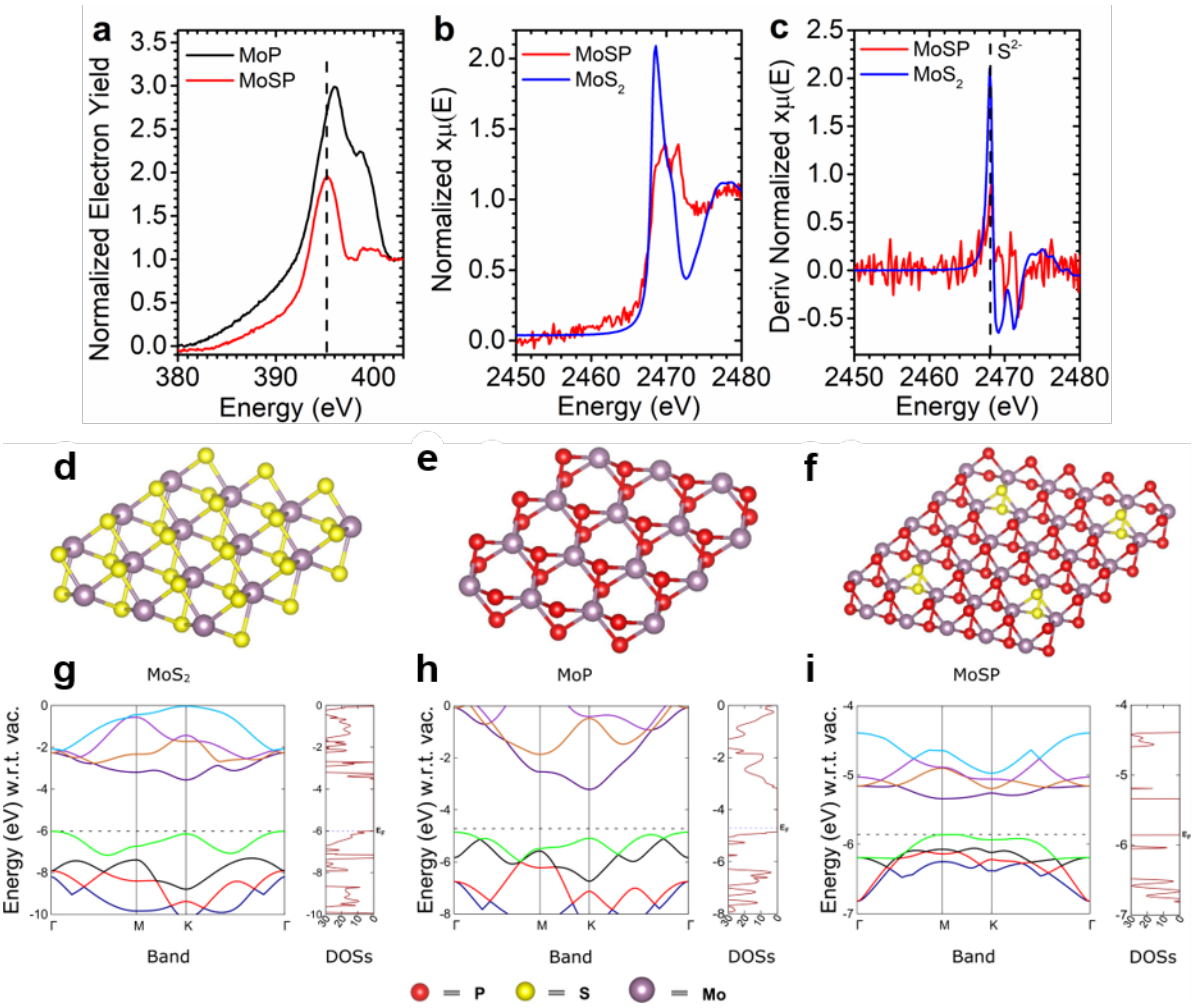

Figure 3. XAS spectra. (a) Mo M_3-edge absorption spectroscopy shows the different 3p-3d hybridization states for MoP (black line) and S-doped MoP (red line). (b) S K-edge normalized and (c) derivative X-ray absorption near edge structure spectra show the MoS_2-like oxidization state of S that is doped in MoP. The optimized structures of (d) MoS_2, (e) MoP, and (f) S-doped MoP, with their respective (g-i) electronic structures, which include the band diagrams and the DOSs.

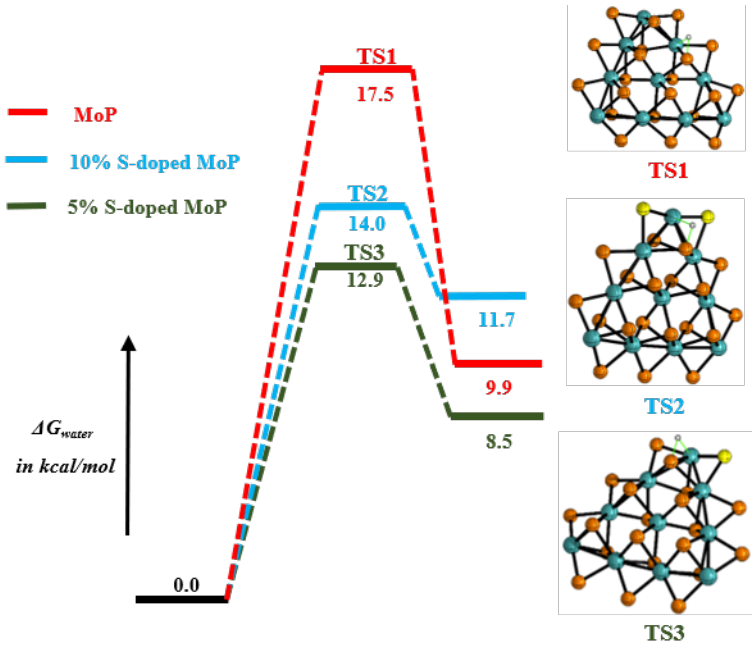

Figure 4. Free energy changes calculated for the rate determining Volmer step over MoP′, 5% S-doped MoPS′, and 10% S-doped MoPS′.